J Mater Sci (2008) 43:6024–6028
DOI 10.1007/s10853-008-2886-5

LETTER

TEM analysis of Cr–Mo–W–B phase in a DS nickel based superalloy

H. R. Zhang · O. A. Ojo

Received: 29 May 2008 / Accepted: 11 July 2008 / Published online: 5 August 2008

Rene 80 is a precipitation hardened nickel-based superalloy, which is widely used to manufacture components of gas turbine engines for aerospace and power generation applications. It is designed to withstand service temperatures of up to 980 °C [1] and possesses remarkable hot corrosion resistance, long-term microstructural stability, and high-temperature strength produced primarily by precipitation hardening by ordered intermetallic $Ni_3(Al,Ti)$ γ' precipitates. Directional solidification (DS) processing of the alloy results in further improvement of its elevated temperature properties and permits the use of a higher service temperature, which improves the thermal efficiency of gas turbines [2–5]. It has been reported that in DS Rene 80, the tensile strength is increased by about 10–15% and the creep rupture life is extended by 2–4 times relative to conventionally cast material [5]. Boron is an essential minor elemental addition to these heat resistant materials primarily to improve their creep rupture properties [3, 4]. Nevertheless, it has been recognized that the mode in which boron exists on grain boundary regions, either in austenitic solid solution form or selectively partitioned into second phase particles, can significantly influence the creep properties of superalloys [6, 7]. Experimental study is crucial in establishing the presence and nature of intergranular borides in multi-component superalloys due to the influence of interfacial elemental segregation that is not generally considered during thermodynamic equilibrium calculations of theoretical models [8]. The objective of this investigation was to perform transmission electron microscopy (TEM) study of heat-treated DS Rene 80 superalloy to understand the nature of boron rich second phase particles present along its grain boundary regions.

The composition of the DS Rene 80 material used in this study was (wt%) 0.2C, 14.1Cr, 9.52Co, 4.0W, 3.98Mo, 0.02Nb, 0.18Fe, 2.9Al, 4.98Ti, 0.028Zr, 0.013B balance nickel. The alloy was subjected to standard solution heat treatment for 2 h at 1200 °C and was subsequently aged at 1025 °C for 16 h. Thin foils from the aged material for TEM study were prepared by mechanical polishing and dimpling to a thickness of less than 10 μm followed by ion milling in a Gatan precision ion polishing system (PIPS). TEM microchemical and crystal-structure analyses were performed in a field emission gun JEOL 2100F scanning transmission electron microscope equipped with Oxford energy dispersive spectrometer (EDS), Gatan imaging filter (GIF) system, and electron energy-loss spectrometer (EELS). High-resolution TEM micrographs were filtered using an inverse fourier fast transform (FFT) program in Gatan Digital Micrography software.

A TEM boron post-edge electron energy loss image of the heat-treated alloy consisting of γ' precipitates and particles of a different phase along the grain boundary and inside the grain identified with arrows is shown in Fig. 1a. Microchemical analysis by X-ray energy dispersive spectroscopy indicated that the particles are rich in Cr, Mo, W, and B (Fig. 1b), and have much different composition from the adjoining regions (Fig. 1c). The presence of boron in the particles was further confirmed by EELS analysis (Fig. 1d) and EELS-based energy filtered transmission electron microscopy (EFTEM) elemental mapping (Fig. 1e). TEM Electron diffraction pattern (EDP) analysis was performed by systematic titling of particle of this phase along certain crystallographic directions to determine its crystal structure. Figure 2a is a [001] zone-axis EDP showing a fourfold symmetry of the phase. Figure 2b and c were obtained by

H. R. Zhang · O. A. Ojo (✉)
Department of Mechanical and Manufacturing Engineering, University of Manitoba, Winnipeg, MB, Canada R3T 5V6
e-mail: ojo@cc.umanitoba.ca

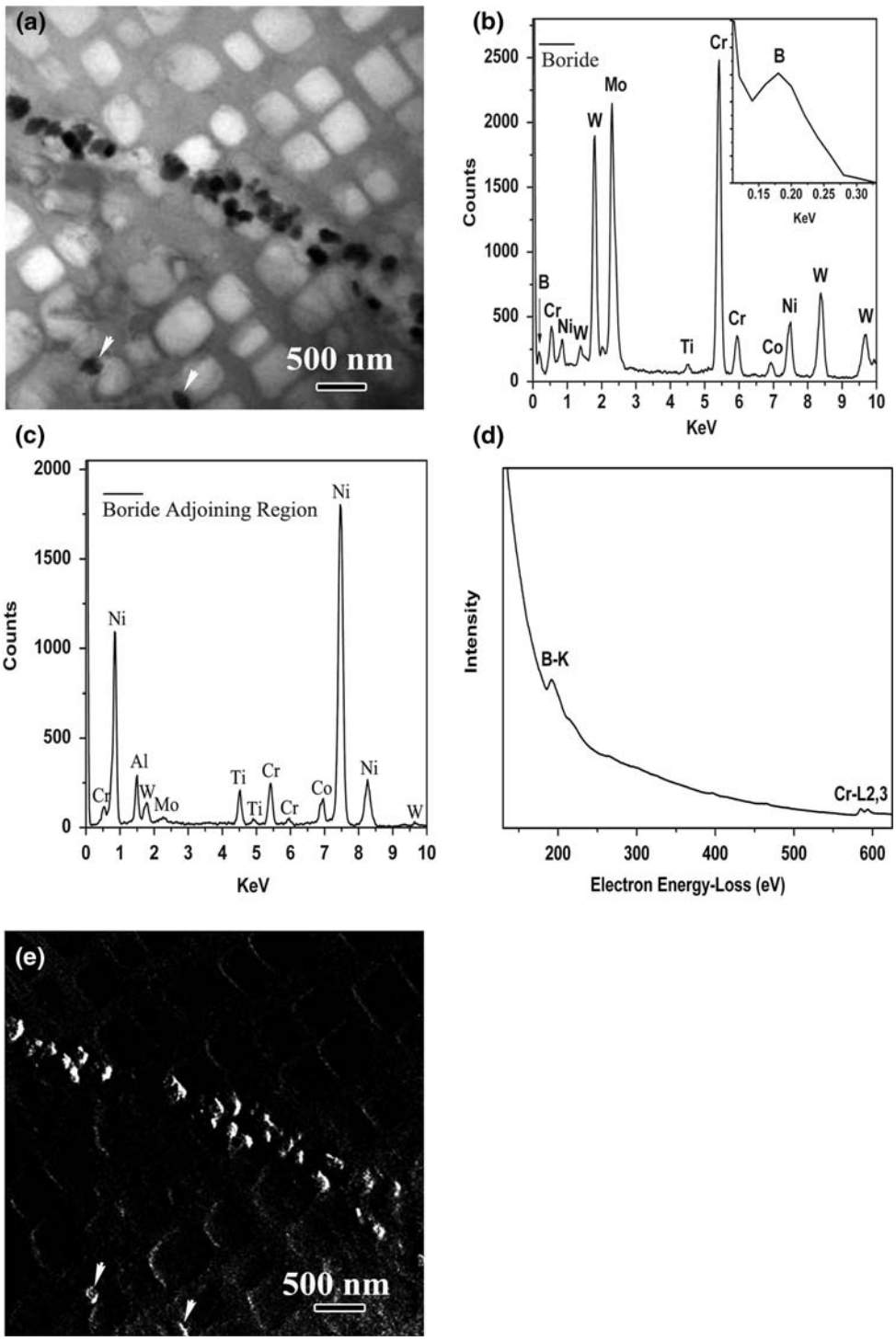

Fig. 1 (**a**) Boron post-edge image obtained using the electrons of 195 eV energy loss with a 10 eV energy-selecting slit showing boride particles along the grain boundary and inside the grain, (**b**) and (**c**) TEM–EDS spectra of the boride particles and the adjoining region, respectively, (**d**) Electron energy-loss spectrum of the boride particles showing the B–K edge peak and (**e**) Boron-map image

tilting around <020>* direction about 28° and 90° away from the [001] zone-axis respectively. The weak $(10\bar{1})$* diffraction spot in Fig. 2b, which has a shorter spacing from the origin compared to that of (110)* diffraction spot, reveals a body-centered tetragonal (BCT) structure of the phase, while the $(10\bar{1})$* diffraction spot was produced by double diffraction. The analysis of EDPs from the particles of this phase indicated them to be Cr_5B_3-type M_5B_3 borides with a BCT structure and lattice parameters of $a = 5.7$ Å, $c = 10.8$ Å, and $c/a = 1.89$. This type of grain boundary boride particle has also been observed in heat-treated IN 738 superalloy [9].

Besides the discrete M_5B_3 boride particles, the boride also formed a continuous film-like morphology along grain boundary, as indicated by arrows in Fig. 3a. Careful analysis showed that the boride particles maintain certain

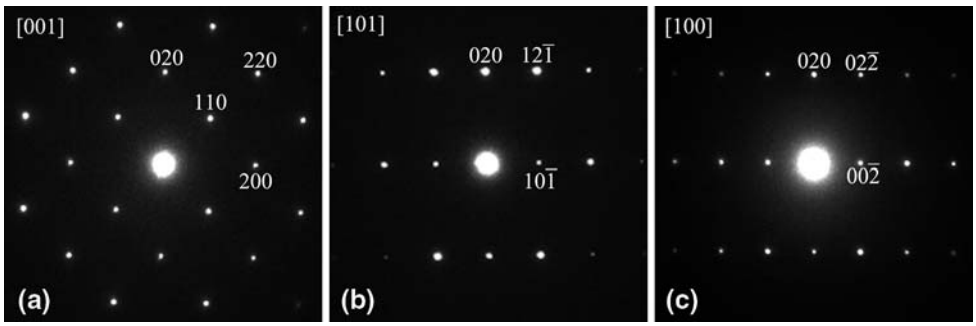

Fig. 2 Selected area electron diffraction patterns obtained from (**a**) [001], (**b**) [101], and (**c**) [100] zone axes of the M_5B_3 boride particles

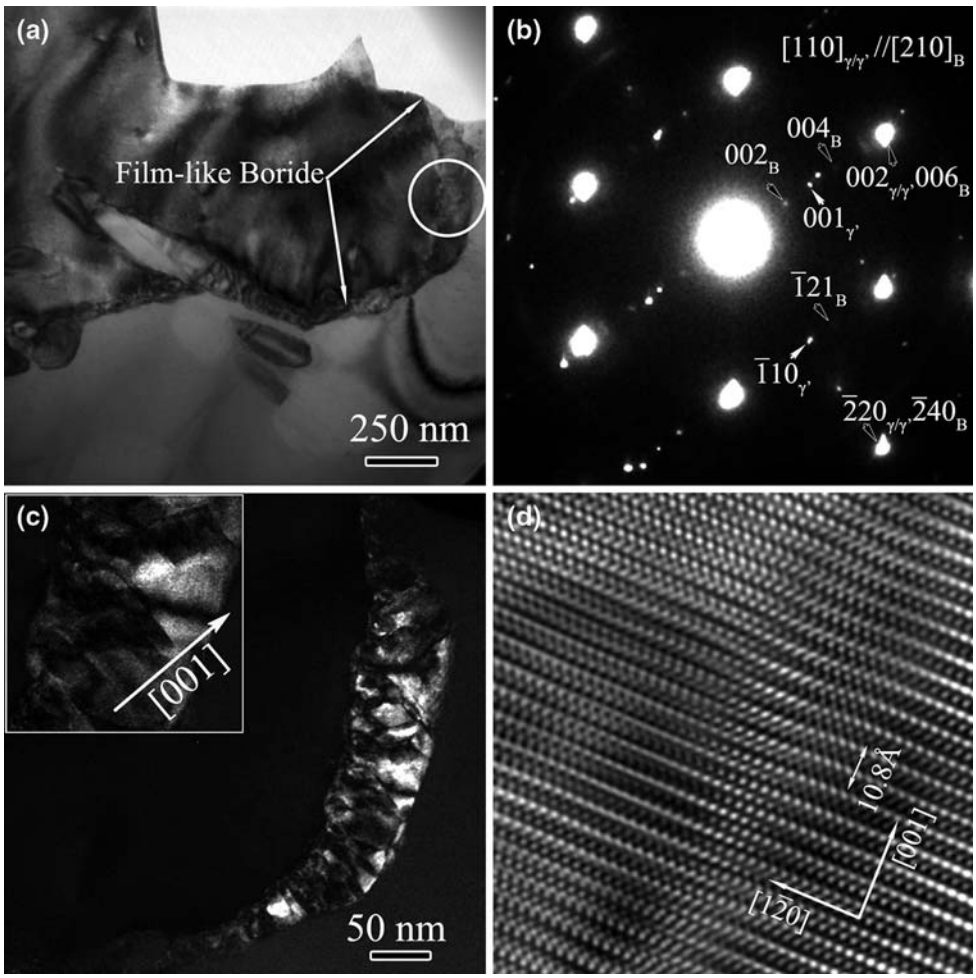

Fig. 3 (**a**) Bright field TEM micrograph showing continuous film-like M_5B_3 boride along the grain boundary region, (**b**) Selected area electron diffraction pattern obtained from the circled area in (**a**) across a grain boundary showing orientation relationship between the intergranular boride and the grain, (**c**) Dark field TEM micrograph showing some structural details of the continuous M_5B_3 boride film, the top left inset is a higher magnification image, (**d**) [210] zone-axis HRTEM image taken from the interface of closely spaced fine particles of M_5B_3 boride film

crystallographic orientation relationship with one of the two grains along the grain boundary. Figure 3b is an EDP taken from the circled area across the grain boundary in Fig. 3a along the $[110]_{\gamma/\gamma'}$ zone-axis of one of the grains. The EDP is composed of three sets of diffraction patterns; from γ' particles (white arrows), M_5B_3 borides (black arrows), and γ matrix sharing the common diffraction spots of γ' precipitate and M_5B_3 (strong spots). The other spots are due to double diffraction from the superimposition. Analysis of the EDPs suggests that the $[110]_{\gamma/\gamma'}$ zone-axes of the γ and γ' phases are parallel to the $[210]_B$ zone-axis of the M_5B_3 boride phase, and that γ and γ' phases maintain crystallographic coherency with the M_5B_3 boride phase. A dark field image in Fig. 3c taken by using the $(002)_B$* reflection in Fig. 3b indicates that the film-like boride was composed of many closely contacted fine particles with identical crystallographic orientation. It should be noted that part of the dark contrast was possibly due to crystal defects. Closer examination at higher magnifications indicated that there were some twin-like (001) planar defects within the fine

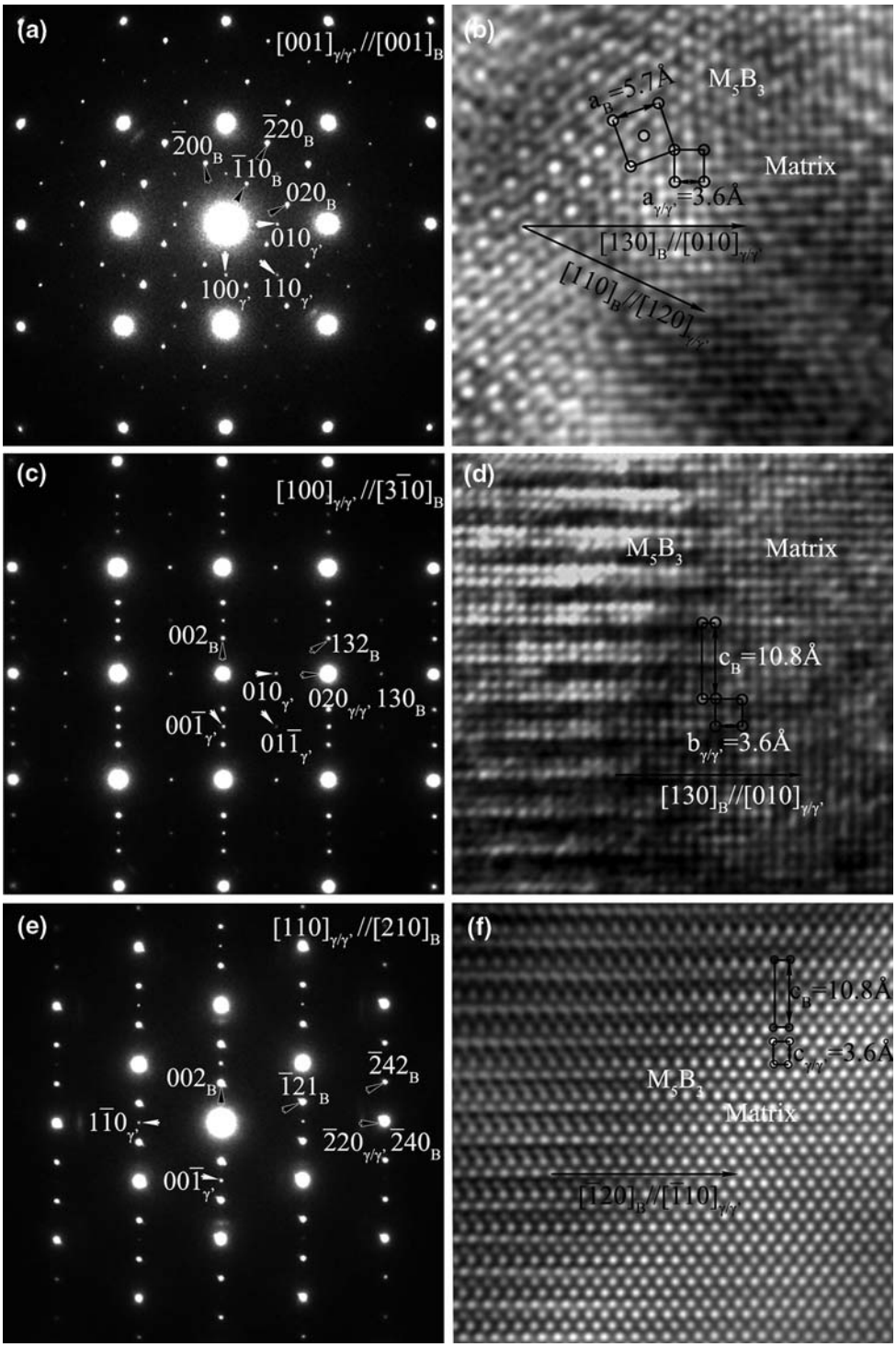

Fig. 4 Selected area electron diffraction patterns and HRTEM images obtained from (**a**) and (**b**) $[001]_{\gamma/\gamma'}//[001]_B$ zone-axis, (**c**) and (**d**) $[100]_{\gamma/\gamma'}//[3\bar{1}0]_B$ zone-axis, and (**e**) and (**f**) $[110]_{\gamma/\gamma'}//[210]_B$ zone-axis, respectively, showing crystallographic orientation relationship between the M_5B_3 boride precipitate, γ matrix, and γ' precipitate

particles, as shown in the top left inset in Fig. 3c. Unfortunately, however, the (001) twin of M_5B_3 boride phase cannot be identified by EDP due to its special crystal symmetry. Another possible reason for the twin-like contrast could also be due to slip. Figure 3d is a high-resolution transmission electron microscopy (HRTEM) image taken from two closely spaced fine particles. The lattice image suggests that the two crystals are closely associated and stacked together with a relative displacement along <001> direction. The left side crystal suggests a twin-like contrast, but it cannot be clearly identified due to possible thickness fluctuation and defect-induced interferences.

In order to better understand the growth mechanism of the M_5B_3 boride phase, detailed EDP and HRTEM analyses

were further performed to study the crystallographic orientation relationship between M_5B_3 boride and the matrix. Figures 4a, c, and e are three composite EDPs of γ matrix, γ' precipitate, and M_5B_3 boride taken from $[001]_{\gamma/\gamma'}//[001]_B$ zone-axis, $[100]_{\gamma/\gamma'}//[3\bar{1}0]_B$ zone-axis, and $[110]_{\gamma/\gamma'}//[210]_B$ zone-axis, respectively. As shown in the figures, the white arrows indicate the weak reflections of ordered γ' phase at the half positions of the strong reflections, and the black arrows indicate the reflections of M_5B_3 boride. All the strong diffraction spots are common reflections of γ matrix, γ' precipitate, and M_5B_3 boride precipitate, which further indicate a coherent crystallographic relationship among the γ matrix, γ' precipitate, and M_5B_3 precipitate. Based on the analyses of the diffraction patterns, the orientation relationship among the γ matrix, γ' precipitate, and M_5B_3 boride precipitate can be determined as

$$(100)_{\gamma/\gamma'}//(3\bar{1}0)_B, \quad [010]_{\gamma/\gamma'}//[130]_B,$$
$$(010)_{\gamma/\gamma'}//(130)_B, \quad [001]_{\gamma/\gamma'}//[001]_B,$$
$$(001)_{\gamma/\gamma'}//(001)_B, \quad [100]_{\gamma/\gamma'}//[3\bar{1}0]_B,$$

The $(001)_{\gamma/\gamma'}$ crystal plane appears to be the habit plane for the formation of M_5B_3 boride. Since (100), (010), and (001) are equivalent crystal planes of cubic γ matrix and γ' precipitate, M_5B_3 boride can precipitate with the three different crystallographic orientation relationships. Figure 4b, d, and f are three corresponding HRTEM images of Figure 4a, c, and e, respectively. The projected unit cells of γ matrix or γ' precipitate, and M_5B_3 boride are indicated by the black frames. These HRTEM images confirm the coherent relationship between the γ matrix or γ' precipitate (right side of the three HRTEM images) and the M_5B_3 boride precipitate (left side of the three HRTEM images).

The growth of the boride phase in an almost continuous grain boundary film can be related to its close orientation relationship with the γ matrix and γ' precipitates. While discrete boride particles can improve creep properties by aiding resistance to grain boundary sliding at high temperatures, semi-continuous or continuous intergranular boride film may in contrast be detrimental by providing low resistance path to crack initiation and/or propagation. Therefore, proper consideration of the presence of these intergranular boride particles in heat-treated DS Rene 80 superalloy is pertinent to creep performance and microstructural response of the material during high temperature exposure and/or processing.

Acknowledgement The authors would like to thank NSERC of Canada for financial support.

References

1. Reed RC (2006) The superalloys—fundamentals and applications, 1st edn. Cambridge University Press, Cambridge, UK, pp 1–29
2. Nakagawa YG, Ohtomo A, Saiga Y (1976) Trans Jpn Inst Met 17:323
3. Allen RE, Sidenstick JE (1980) Proceedings of ASME Century 2 Aerospace Conference (Paper No. 80-C2/AERO-10), San Francisco, California, 13–15 Aug 1980, p 1
4. Neidel A, Riesenbeck S, Ulrich T, Volker J, Yao C (2005) Materialpruefung Mater Test 47(10):553
5. Raguet M, Antolovich SD, Payne RK (1984) In: Gell M et al (eds) Proceedings of superalloys conference. TMS, Seven Springs, PA, p 231
6. Garosshen TG, Tillman TD, McCarthy GP (1987) Metall Trans 18A:69
7. Jena AK, Chaturvedi MC (1984) J Mater Sci 19:3121. doi: 10.1007/BF00549796
8. Tancret F, Bhadeshia HKDH (2003) Mater Sci Tech 19:291. doi: 10.1179/026708303225009797
9. Zhang HR, Ojo OA, Chaturvedi MC (2008) Scr Mater 58:167. doi: 10.1016/j.scriptamat.2007.09.049